

Intertwined Quantum Phase Transitions in the Zr Isotopes

N. Gavrielov* and A. Leviatan†

Racah Institute of Physics, The Hebrew University, Jerusalem 91904, Israel

F. Iachello‡

*Center for Theoretical Physics, Sloane Physics Laboratory,
Yale University, New Haven, Connecticut 06520-8120, USA*

(Dated: November 13, 2021)

We explore the situation of intertwined quantum phase transitions (IQPTs), for which a QPT involving a crossing of two configurations is accompanied by a shape evolution of each configuration with its own separate QPT. We demonstrate the relevance of IQPTs to the Zr isotopes, with such coexisting Type I and Type II QPTs, and ground state shapes changing from spherical to prolate axially deformed and finally to gamma-unstable. Evidence for this scenario is provided by a detailed comparison with experimental data, using a definite symmetry-based conceptual framework.

I. INTRODUCTION

Quantum Phase transitions (QPT) have in recent years become of great interest in a variety of fields [1]. In particular, they have been the subject of many investigations in nuclear physics [2–5], where they were originally introduced [6, 7]. In this field, most of the attention has been devoted to shape phase transitions in a single configuration, described by a single Hamiltonian,

$$\hat{H} = (1 - \xi) \hat{H}_1 + \xi \hat{H}_2, \quad (1)$$

where ξ is the control parameter. As ξ changes from 0 to 1, the symmetry and equilibrium shape of the system change from those of \hat{H}_1 to those of \hat{H}_2 . For sake of clarity, we denote these phase transitions Type I.

A different type of phase transitions occurs when two (or more) configurations coexist [8]. In this case, the quantum Hamiltonian has a matrix form [9]

$$\hat{H} = \begin{bmatrix} \hat{H}_A(\xi^A) & \hat{W}(\omega) \\ \hat{W}(\omega) & \hat{H}_B(\xi^B) \end{bmatrix}, \quad (2)$$

where the index A, B denotes the two configurations and \hat{W} denotes their coupling. We call for sake of clarity these phase transitions Type II [9], to distinguish them from those of a single configuration [10]. The two types of QPTs are usually discussed separately and both have been established in nuclei, *e.g.*, Type I QPT in the neutron number 90 region for Nd-Sm-Gd isotopes, and Type II QPT in nuclei near shell closure, *e.g.*, in the light Pb-Hg isotopes, with strong mixing between the two configurations. In the present work, we explore a situation where the two crossing configurations, although coupled, still maintain individually a pronounced shape evolution with nucleon number. We refer to such a scenario as intertwined quantum phase transitions (IQPTs) in the

sense that Type I and Type II coexist, and show empirical evidence for it in transitional nuclei, analyzed in a physically transparent symmetry-based framework.

II. ALGEBRAIC APPROACH TO QPTS

A variety of methods have been used to study shape phase transitions in nuclei. We prefer here to use algebraic models, in which both Hamiltonians, \hat{H}_A and \hat{H}_B , and their coupling, \hat{W} , are written in terms of the Interacting Boson Model (IBM) [11], with bosons representing valence nucleon pairs counted from the nearest closed shells. This provides a simple tractable shell-model-inspired framework, where global trends of structure and symmetries can be clearly identified and diversity of observables calculated. Other microscopic but computationally demanding approaches include mean-field methods, both non-relativistic [12] and relativistic [13], and very recently the Monte-Carlo shell-model (MCSM) [14]. In this paper, we focus on the ${}_{40}\text{Zr}$ isotopes and find a complex variety of phase transitions both of Type I and Type II coexist, thus exemplifying IQPTs. These isotopes have been very recently the subject of several experimental investigations [15–21].

To be specific, we use the configuration mixing model (IBM-CM) of [22], and write the Hamiltonian not in matrix form, but rather in the equivalent form

$$\hat{H} = \hat{H}_A^{(N)} + \hat{H}_B^{(N+2)} + \hat{W}^{(N,N+2)}, \quad (3)$$

where $\hat{O}^{(N)} = \hat{P}_N^\dagger \hat{O} \hat{P}_N$ and $\hat{O}^{(N,N')} = \hat{P}_N^\dagger \hat{O} \hat{P}_{N'}$, for an operator \hat{O} , with \hat{P}_N , a projection operator onto the $[N]$ boson space. Here $\hat{H}_A^{(N)}$ represents the so-called normal (N boson space) configuration and $\hat{H}_B^{(N+2)}$ represents the so-called intruder ($N+2$ boson space) configuration, which we have assumed, as in [23] where a similar calculation was done for the ${}_{42}\text{Mo}$ isotopes, to be a proton excitation across the subshell closure at proton number 40 (see Fig. 1 of [23]). The explicit form of these Hamil-

* noam.gavrielov@mail.huji.ac.il

† ami@phys.huji.ac.il

‡ francesco.iachello@yale.edu

TABLE I. Parameters of the IBM-CM Hamiltonian, Eq. (4), are in MeV and χ is dimensionless. The first row of the Table lists the number of neutrons, and particle-bosons ($N, N + 2$) or hole-bosons ($\bar{N}, \bar{N} + 2$) in the (A, B) configurations.

	52(1, 3)	54(2, 4)	56(3, 5)	58(4, 6)	60(5, 7)	62(6, 8)	64(7, 9)	66(8, 10)	68($\bar{7}, \bar{9}$)	70($\bar{6}, \bar{8}$)
$\epsilon_d^{(A)}$	0.7	0.8	1.82	1.75	1.2	1.2	1.2	1.2	1.2	1.2
$\kappa^{(A)}$	-0.005	-0.005	-0.005	-0.007	-0.006	-0.006	-0.006	-0.006	-0.006	-0.006
$\epsilon_d^{(B)}$	0.35	0.37	0.6	0.45	0.3	0.15	0	0	0	0.15
$\kappa^{(B)}$	-0.02	-0.02	-0.015	-0.02	-0.02	-0.025	-0.0275	-0.03	-0.0275	-0.025
$\kappa'^{(B)}$	0.01	0.01	0.01	0.01	0.0075	0.01	0.0125	0.0125	0.0125	0.01
χ	-0.6	-0.6	-0.6	-0.6	-1.0	-1.0	-0.75	-0.25	-0.25	0
$\Delta_p^{(B)}$	1.6	1.6	1.84	1.43	0.8	0.8	0.8	0.8	0.8	0.8
ω	0.1	0.1	0.02	0.02	0.02	0.02	0.02	0.02	0.02	0.02

tonians is

$$\hat{H}_A = \epsilon_d^{(A)} \hat{n}_d + \kappa^{(A)} \hat{Q}_\chi \cdot \hat{Q}_\chi, \quad (4a)$$

$$\hat{H}_B = \epsilon_d^{(B)} \hat{n}_d + \kappa^{(B)} \hat{Q}_\chi \cdot \hat{Q}_\chi + \kappa'^{(B)} \hat{L} \cdot \hat{L} + \Delta_p^{(B)}, \quad (4b)$$

where the quadrupole operator is defined as $\hat{Q}_\chi = d^\dagger s + s^\dagger \tilde{d} + \chi(d^\dagger \times \tilde{d})^{(2)}$. In Eq. (4b), $\Delta_p^{(B)}$ is the off-set between the normal and intruder configurations, where the index p denotes the fact that this is a proton excitation. The mixing term has the form [11, 22]

$$\hat{W} = [\omega_d (d^\dagger \times d^\dagger)^{(0)} + \omega_s (s^\dagger)^2] + \text{H.c.}, \quad (5)$$

where, for simplicity, a single parameter $\omega = \omega_s = \omega_d$ is used. Hamiltonians of the above form, have been used extensively for studying coexistence phenomena in nuclei [22–31]. The resulting eigenstates $|\Psi; L\rangle$ with angular momentum L , are linear combinations of the wave functions, Ψ_A and Ψ_B , in the two spaces $[N]$ and $[N + 2]$,

$$|\Psi; L\rangle = a|\Psi_A; [N], L\rangle + b|\Psi_B; [N + 2], L\rangle, \quad (6)$$

with $a^2 + b^2 = 1$. We note here that one of the advantages of the algebraic method is that one can also study phase transitions semi-classically by introducing intrinsic states [32, 33] and constructing the corresponding energy functional (or potential function). For a single configuration, the latter is a scalar function of the quadrupole variables, β and γ [11]. When two configurations coexist, the energy functional becomes a matrix. Diagonalization of this two-by-two matrix produces the so-called eigenpotentials, $E_\pm(\beta, \gamma)$ [9, 34, 35].

III. QPTS IN THE ZIRCONIUM CHAIN

The IBM-CM framework described above has been previously employed to the Zr chain in [30], where the Hamiltonian parameters were determined by a mapping between microscopic-derived and IBM energy surfaces. Due to the mean-field nature of this procedure, the Hamiltonian obtained exhibited noticeable deviations from the data in the vicinity of the critical point. In the

current study, we adapt a different approach as in [23–28], with parameters determined from a combined fit to the data on spectra and $E2$ transitions for the states of $^{92-110}\text{Zr}$ shown in Fig. 1, allowing a gradual change between adjacent isotopes, but taking into account the proposed shell-model interpretation for the structure evolution in this region [36–38]. The Hamiltonian parameters used are given in Table I and are consistent with those of previous calculations in this mass region [23–25], where a similar fit procedure was employed. It should be noted that beyond the middle of the shell at neutron number 66, bosons are replaced by boson holes [11], and denoted by a bar over their number, and a symmetry about mid-shell was imposed on all parameters (except χ), in accord with microscopic aspects of the IBM [39]. Apart from some fluctuations due to the subshell closure at neutron number 56 (the filling of the $2d_{5/2}$ orbital [36]), the values of the parameters are a smooth function of neutron number and, in some cases, a constant. A notable exception is the sharp decrease by 1 MeV of the energy off-set parameter $\Delta_p^{(B)}$ beyond neutron number 56. Such a behavior was observed for the Mo and Ge chains [23–25] and, as noted in [23], it reflects the effects of the isoscalar residual interaction, V_{pn} , between protons and neutrons occupying the partner orbitals $1g_{9/2}$ and $1g_{7/2}$, which is the established mechanism for descending cross shell-gap excitations and onset of deformation in this region [37, 38]. This trend in $\Delta_p^{(B)}$ agrees with shell model estimates for the monopole correction of V_{pn} [40]. The parameter ω (5) is determined from $E2$ transitions in-between configurations, and is constant except for $^{92,94}\text{Zr}$ where the normal configuration space is small ($N = 1, 2$). Fine-tuning the parameters for individual isotopes can improve the fit, but the main conclusions of the analysis, to be reported below, are not changed.

In Fig. 1 we show a comparison between experimental and calculated levels. One can see here a rather complex structure. In the region between neutron number 50 and 56, there appear to be two configurations, one spherical (seniority-like), (A), and one weakly deformed, (B), as evidenced by the ratio $R_{4/2}$, which is at 52-56, $R_{4/2}^{(A)} \cong 1.6$ and $R_{4/2}^{(B)} \cong 2.3$. From neutron number 58,

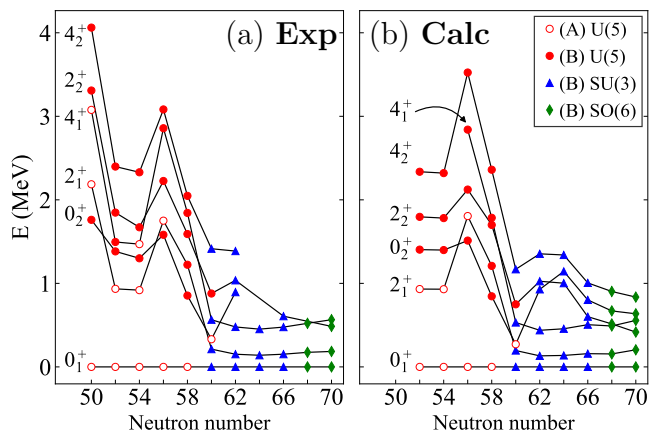


FIG. 1. Comparison between (a) experimental [19, 42] and (b) calculated energy levels 0_1^+ , 2_1^+ , 4_1^+ , 0_2^+ , 2_2^+ , 4_2^+ . Empty (filled) symbols indicate a state dominated by the normal A -configuration (intruder B -configuration), with assignments based on the decomposition of Eq. (6). Note that the calculated values start at neutron number 52, while the experimental values include the closed shell at 50.

there is a pronounced drop in energy for the states of configuration B and at 60, the two configurations exchange their role indicating a Type II QPT. At this stage, the intruder configuration (B) appears to be at the critical point of a U(5)-SU(3) Type I QPT, as evidenced by the low value of the excitation energy of the first excited 0^+ state of this configuration (the 0_3^+ state in ^{100}Zr shown in Fig. 3). The same situation is seen in the ^{62}Sm and ^{64}Gd isotopes at neutron number 90 [11, 41]. Beyond neutron number 60, the intruder configuration (B) is strongly deformed, as evidenced by the small value of the excitation energy of the state 2_1^+ , $E_{2_1^+} = 139.3$ keV and by the ratio $R_{4/2}^{(B)} = 3.24$ in ^{104}Zr . At still larger neutron number 66, the ground state band becomes γ -unstable (or triaxial) as evidenced by the close energy of the states 2_2^+ and 4_1^+ , $E_{2_2^+} = 607.0$ keV, $E_{4_1^+} = 476.5$ keV, in ^{106}Zr , and especially by the recent results $E_{4_1^+} = 565$ keV and $E_{2_2^+} = 485$ keV in ^{110}Zr [19], a signature of the SO(6) symmetry. In this region, the ground state configuration undergoes a crossover from SU(3) to SO(6).

The above spectral analysis suggests a situation of co-existing Type I and Type II QPTs, which is the defining property of IQPTs. In order to understand the nature of these phase transitions, one needs to study the behavior of the order parameters. In the present study, the latter involve the expectation value of \hat{n}_d in the ground state wave function, $|\Psi; L = 0_1^+\rangle$ and in its Ψ_A and Ψ_B components (6), denoted by $\langle \hat{n}_d \rangle_{0_1^+}$, $\langle \hat{n}_d \rangle_A$, $\langle \hat{n}_d \rangle_B$, respectively. $\langle \hat{n}_d \rangle_A$ and $\langle \hat{n}_d \rangle_B$ portray the shape-evolution in configuration (A) and (B), respectively, and $\langle \hat{n}_d \rangle_{0_1^+} = a^2 \langle \hat{n}_d \rangle_A + b^2 \langle \hat{n}_d \rangle_B$ contains information on the normal-intruder mixing. Fig. 2(a) shows the evolution along the Zr chain of these order parameters ($\langle \hat{n}_d \rangle_A$, $\langle \hat{n}_d \rangle_B$

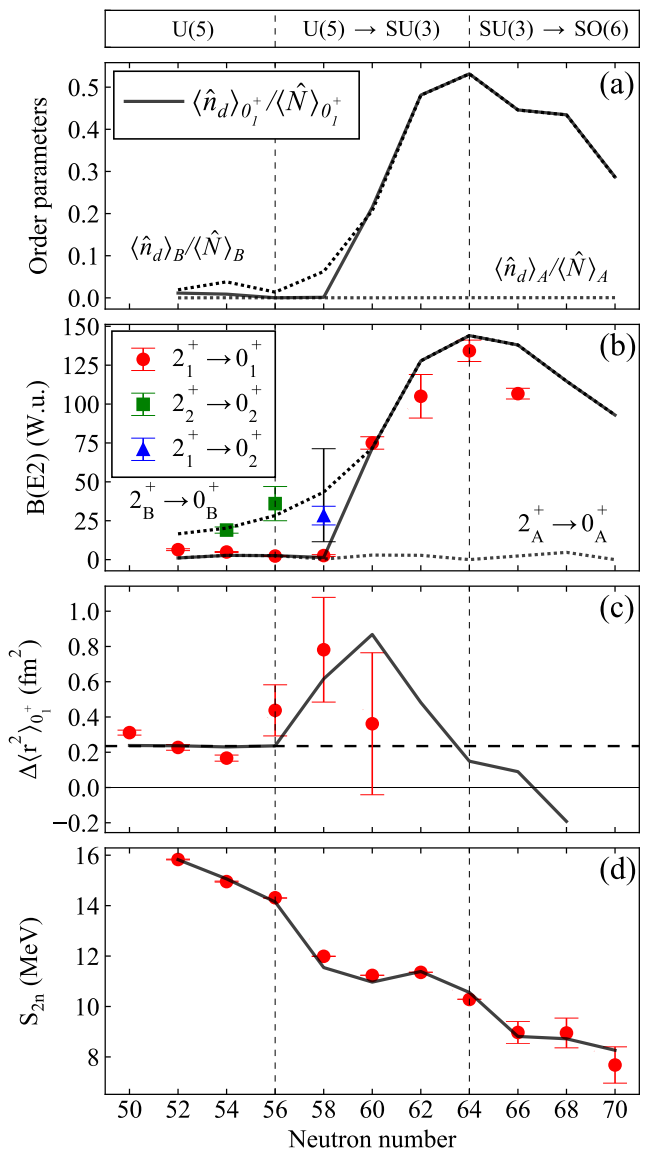


FIG. 2. Evolution of order parameters and of observables along the Zr chain. Symbols (solid lines) denote experimental data (calculated results). Relevant parameters are given in the text. (a) Order parameters (see text for details). (b) $B(E2)$ values in Weisskopf units (W.u.). Data taken from [15–18, 20, 21, 42]. Dotted lines denote calculated $E2$ transitions within a configuration. (c) Isotope shift, $\Delta \langle \hat{r}^2 \rangle_{0_1^+}$ in fm^2 . Data taken from [43]. The horizontal dashed line at 0.235 fm^2 represents the smooth behavior in $\Delta \langle \hat{r}^2 \rangle_{0_1^+}$ due to the $A^{1/3}$ increase of the nuclear radius. (d) Two-neutron separation energies, S_{2n} , in MeV. Data taken from AME2016 [44].

in dotted and $\langle \hat{n}_d \rangle_{0_1^+}$ in solid lines), normalized by the respective boson numbers, $\langle \hat{N} \rangle_A = N$, $\langle \hat{N} \rangle_B = N + 2$, $\langle \hat{N} \rangle_{0_1^+} = a^2 N + b^2 (N + 2)$. Configuration (A) is seen to be spherical for all neutron numbers considered. In contrast, configuration (B) is weakly-deformed for neutron

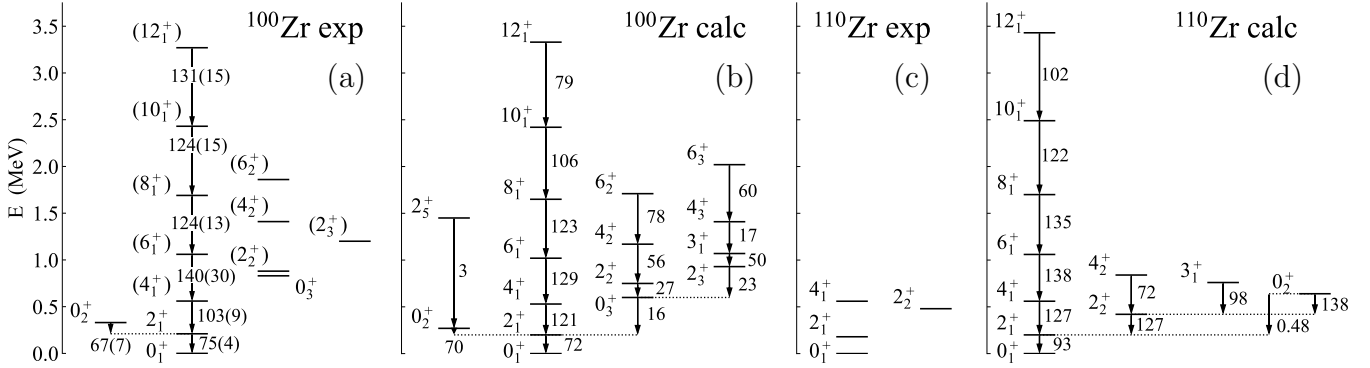


FIG. 3. Experimental and calculated energy levels in MeV and $E2$ rates in W.u. for ^{100}Zr [panels (a)-(b)], and ^{110}Zr [panels (c)-(d)].

number 52-58. One can see here clearly a jump between neutron number 58 and 60 from configuration (A) to configuration (B), indicating a 1st order Type II phase transition [9], a further increase at neutron numbers 60-64 indicating a U(5)-SU(3) Type I phase transition, and, finally, there is a decrease at neutron number 66, due in part to the crossover from SU(3) to SO(6) and in part to the shift from boson particles to boson holes after the middle of the major shell 50-82. $\langle \hat{n}_d \rangle_{0_1^+}$ is close to $\langle \hat{n}_d \rangle_A$ for neutron number 52-58 and coincides with $\langle \hat{n}_d \rangle_B$ at 60 and above, consistent with a high degree of purity with respect to configuration-mixing. These conclusions are stressed by an analysis of other observables, in particular, the $B(E2)$ values. Adapted to two configurations, the $E2$ operator reads $\hat{T}(E2) = e^{(A)} \hat{Q}_\chi^{(N)} + e^{(B)} \hat{Q}_\chi^{(N+2)}$, with $\hat{Q}_\chi^{(N)} = \hat{P}_N^\dagger \hat{Q}_\chi \hat{P}_N$ and $\hat{Q}_\chi^{(N+2)} = \hat{P}_{N+2}^\dagger \hat{Q}_\chi \hat{P}_{N+2}$. The boson effective charges $e^{(A)} = 0.9$ and $e^{(B)} = 2.24$ (W.u.)^{1/2} are determined from the $2^+ \rightarrow 0^+$ transition within each configuration, and χ is the same parameter as in the Hamiltonian (4). As shown in Fig. 2(b), the calculated $B(E2)$'s agree with the empirical values and follow the same trends as the respective order parameters.

Further evidence can be obtained from an analysis of the isotope shift $\Delta \langle \hat{r}^2 \rangle_{0_1^+} = \langle \hat{r}^2 \rangle_{0_1^+; A+2} - \langle \hat{r}^2 \rangle_{0_1^+; A}$, where $\langle \hat{r}^2 \rangle_{0_1^+}$ is the expectation value of \hat{r}^2 in the ground state 0_1^+ . In the IBM-CM the latter is given by $\langle \hat{r}^2 \rangle = r_c^2 + \alpha N_v + \eta [\langle \hat{n}_d^{(N)} \rangle + \langle \hat{n}_d^{(N+2)} \rangle]$, where r_c^2 is the square radius of the closed shell, N_v is half the number of valence particles, and η is a coefficient that takes into account the effect of deformation [11, 45]. $\Delta \langle \hat{r}^2 \rangle_{0_1^+}$ depends on two parameters, $\alpha = 0.235$, $\eta = 0.264$ fm², whose values are fixed by the procedure of Ref [45]. $\Delta \langle \hat{r}^2 \rangle_{0_1^+}$ should increase at the transition point and decrease and, as seen in Fig. 2(c), it does so, although the error bars are large and no data are available beyond neutron number 60. (In the large N limit, this quantity, proportional to the derivative of the order parameter $\langle \hat{n}_d \rangle_{0_1^+}$, diverges at the critical point). Similarly, the two-neutron separation energies S_{2n} can be written as [11], $S_{2n} = -\tilde{A} - \tilde{B} N_v \pm S_{2n}^{\text{def}} - \Delta_n$,

where S_{2n}^{def} is the contribution of the deformation, obtained by the expectation value of the Hamiltonian in the ground state 0_1^+ . The + sign applies to particles and the - sign to holes, and Δ_n takes into account the neutron subshell closure at 56, $\Delta_n = 0$ for 50-56 and $\Delta_n = 2$ MeV for 58-70. The value of Δ_n is taken from Table XII of [46] and $\tilde{A} = -16.5$, $\tilde{B} = 0.758$ MeV are determined by a fit to binding energies of $^{92,94,96}\text{Zr}$. The calculated S_{2n} , shown in Fig. 2(d), displays a complex behavior. Between neutron number 52 and 56 it is a straight line, as the ground state is spherical (seniority-like) configuration (A). After 56, it first goes down due to the subshell closure at 56, then it flattens as expected from a 1st order Type I QPT (see, for example the same situation in the ^{62}Sm isotopes [41]). After 62, it goes down again due to the increasing of deformation and finally it flattens as expected from a crossover from SU(3) to SO(6).

We note that our calculations describe the experimental data in the entire range $^{92-110}\text{Zr}$ very well. A full account is given in [47]. Here we show only two examples, ^{100}Zr and ^{110}Zr . ^{100}Zr is near the critical point of both Type I and Type II QPT and yet our description of energy levels and $B(E2)$ values is excellent, Fig. 3(a)-(b). The ground state band, configuration (B), appears to have features of the so-called X(5) symmetry [48], while the spherical configuration (A) has now become the excited band 0_2^+ . ^{110}Zr , Fig. 3(c)-(d), appears instead to be an excellent example of SO(6) symmetry [49], although few experimental data are available. In general, the results of the current phenomenological study resemble those obtained in the microscopic approach of the MCSM [14] (which focuses on spectra and $E2$ rates), however, there are some noticeable differences. Specifically, the replacement γ -unstable \rightarrow triaxial and the inclusion of more than two configurations in the MCSM. The spherical state in ^{100}Zr is identified in the MCSM as 0_4^+ , in contrast to 0_2^+ in the current calculation and the data. Both calculations show a large jump in $B(E2; 2_1^+ \rightarrow 0_1^+)$, between ^{98}Zr and ^{100}Zr , typical of a 1st order QPT. This is in contrast with mean-field based calculations [30, 50, 51], which due to their character

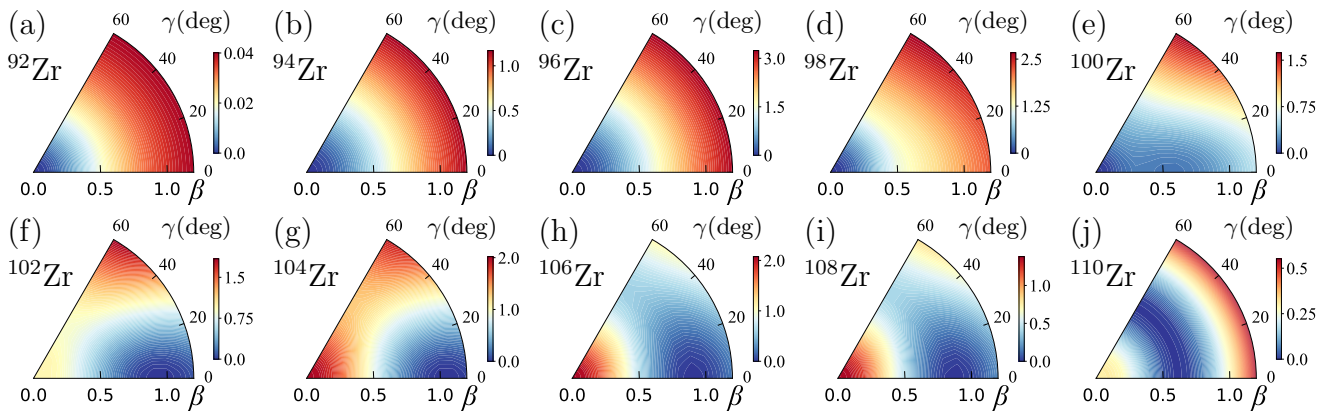


FIG. 4. Contour plots in the (β, γ) plane of the lowest eigen-potential surface, $E_-(\beta, \gamma)$, for the $^{92-110}\text{Zr}$ isotopes.

smooth out the phase transitional behavior, and show no such jump at the critical point of the QPT (see Fig. 2 of [21]). The observed peak in $B(E2; 2_1^+ \rightarrow 0_1^+)$ for ^{104}Zr , is reproduced by the current calculation but not by the MCSM.

As mentioned above, one of the main advantages of the algebraic method is that one can do both a quantum and a classical analysis. In Fig. 4, we show the calculated lowest eigen-potential $E_-(\beta, \gamma)$. These classical potentials confirm the quantum results, as they show a transition from spherical ($^{92-98}\text{Zr}$), Fig. 4(a)-(d), to a flat-bottomed potential at ^{100}Zr , Fig. 4(e), to axially deformed ($^{102-104}\text{Zr}$), Fig. 4(f)-(g), and finally to γ -unstable ($^{106-110}\text{Zr}$), Fig. 4(h)-(j).

IV. CONCLUSIONS

In this article, we have calculated the spectra and several other observables for the entire chain of $_{40}\text{Zr}$ isotopes, from neutron number 52 to 70, in the framework of the IBM-CM. The results of the comprehensive analysis suggest that IQPTs appear to be manifested empirically in these isotopes. The latter exhibit a complex phase structure with two configurations, one spherical (A) and the other (B) undergoing first a QPT $U(5)$ - $SU(3)$ and then a crossover $SU(3)$ - $SO(6)$.

These shape-changing Type I QPTs occur simultaneously with a configuration-changing Type II QPT, in which the normal and intruder configurations cross, a characteristic pattern of IQPTs. Further details of our results, including the calculation of spectra and transition rates in all the $^{92-110}\text{Zr}$ isotopes and of other quantities not reported here, will be given in a forthcoming publication based on [47]. Our method of calculation could also be applied to the $_{38}\text{Sr}$ isotopes, which show similar features, and we are planning to do so in a future publication. The present work provides the first evidence for intertwined quantum phase transitions in nuclear physics and may stimulate research for this type of phase transitions in other fields of physics.

ACKNOWLEDGMENTS

This work was supported in part by U.S. DOE under Grant No. DE-FG02-91ER-40608 and by the US-Israel Binational Science Foundation Grant No. 2016032. We thank R. F. Casten for fruitful discussions. Upon completion of this work, we have learned from J. E. García-Ramos, of another ongoing calculation for the Zr isotopes in the IBM-CM framework.

-
- [1] See, for example, *Understanding Quantum Phase Transitions*, L. Carr, ed., (CRC Press, Boca Raton, FL, 2011).
 [2] P. Cejnar and J. Jolie, *Prog. Part. Nucl. Phys.* **62**, 210 (2009).
 [3] P. Cejnar, J. Jolie and R. F. Casten, *Rev. Mod. Phys.* **82**, 2155 (2010).
 [4] F. Iachello and M. A. Caprio, in *Understanding Quantum Phase Transitions*, L. Carr, ed., (CRC Press, Boca Raton, FL, 2011), pp. 673-700.
 [5] F. Iachello, *Rivista del Nuovo Cimento*, Vol. **34**, 617 (2011).
 [6] R. Gilmore and D. H. Feng, *Phys. Lett. B* **76**, 26 (1978).
 [7] R. Gilmore, *J. Math. Phys.* **20**, 891 (1979).
 [8] K. Heyde and J. L. Wood, *Rev. Mod. Phys.* **83**, 1467 (2011).
 [9] A. Frank, P. Van Isacker and F. Iachello, *Phys. Rev. C* **73**, 061302(R) (2006).
 [10] K. Heyde, J. Jolie, R. Fossion, S. De Baerdemacker and V. Hellemans, *Phys. Rev. C* **69**, 054304 (2004).
 [11] F. Iachello and A. Arima, *The Interacting Boson Model*, (Cambridge University Press, Cambridge, 1987).

- [12] L. M. Robledo, R. R. Rodríguez-Guzmán and P. Sarriguren, *Phys. Rev. C* **78**, 034314 (2008).
- [13] T. Nikšić, D. Vretenar, G. A. Lalazisis and P. Ring, *Phys. Rev. Lett.* **99**, 092502 (2007).
- [14] T. Togashi, Y. Tsunoda, T. Otsuka and N. Shimizu, *Phys. Rev. Lett.* **117**, 172502 (2016).
- [15] A. Chakraborty, E.E. Peters, B.P. Crider, C. Andreoiu, P.C. Bender, D.S. Cross, G. A. Demand, A.B. Garnsworthy, P.E. Garrett *et al.*, *Phys. Rev. Lett.* **110**, 022504 (2013).
- [16] F. Browne *et al.*, *Phys. Lett. B* **750**, 448 (2015).
- [17] C. Kremer, S. Aslanidou, S. Bassauer, M. Hilcker, A. Krugmann, P. von Neumann-Cosel, T. Otsuka, N. Pietralla, V. Yu. Ponomarev *et al.*, *Phys. Rev. Lett.* **117**, 172503 (2016).
- [18] S. Ansari, J.M. Régis, J. Jolie, N. Saed-Samii, N. Warr, W. Korten, M. Zielińska, M.-D. Salsac, A. Blanc *et al.*, *Phys. Rev. C* **96**, 054323 (2017).
- [19] N. Paul *et al.*, *Phys. Rev. Lett.* **118**, 032501 (2017).
- [20] W. Witt, V. Werner, N. Pietralla, M. Albers, A.D. Ayangeakaa, B. Bucher, M. P. Carpenter, D. Cline, H.M. David *et al.*, *Phys. Rev. C* **98**, 041302(R) (2018).
- [21] P. Singh, W. Korten, T.W. Hagen, A. Görgen, L. Greife, M.-D. Salsac, F. Farget, E. Clément, G. de France *et al.*, *Phys. Rev. Lett.* **121**, 192501 (2018).
- [22] P. D. Duval and B. R. Barrett, *Phys. Lett. B* **100**, 223 (1981); *Nucl. Phys. A* **376**, 213 (1982).
- [23] M. Sambataro and G. Molnár, *Nucl. Phys. A* **376**, 201 (1982).
- [24] P. D. Duval, D. Goutte and M. Vergnes, *Phys. Lett. B* **124**, 297 (1983).
- [25] E. Padilla-Rodala, O. Castaños, R. Bijker and A. Galindo-Uribarri, *Rev. Mex. Fis.* **52**, 57 (2006).
- [26] R. Fossion, K. Heyde, G. Thiamova and P. Van Isacker, *Phys. Rev. C* **67**, 024306 (2003).
- [27] J. E. García-Ramos, V. Hellemans and K. Heyde, *Phys. Rev. C* **84**, 014331 (2011).
- [28] J. E. García-Ramos and K. Heyde, *Phys. Rev. C* **89**, 014306 (2014); *Phys. Rev. C* **92**, 034309 (2015).
- [29] K. Nomura, T. Otsuka and P. Van Isacker, *J. Phys. G* **43**, 024008 (2016).
- [30] K. Nomura, R. Rodríguez-Guzmán and L. M. Robledo, *Phys. Rev. C* **94**, 044314 (2016).
- [31] A. Leviatan, N. Gavrielov, J. E. García-Ramos and P. Van Isacker, *Phys. Rev. C* **98**, 031302(R) (2018).
- [32] J. N. Ginocchio and M. W. Kirson, *Phys. Rev. Lett.* **44**, 1744 (1980).
- [33] A. E. L. Dieperink, O. Scholten and F. Iachello *Phys. Rev. Lett.* **44**, 1747 (1980).
- [34] A. Frank, P. Van Isacker and C. E. Vargas, *Phys. Rev. C* **69**, 034323 (R) (2004).
- [35] V. Hellemans, P. Van Isacker, S. De Baerdemacker and K. Heyde, *Nucl. Phys. A* **789**, 164 (2007).
- [36] N. Auerbach and I. Talmi, *Nucl. Phys. A* **64**, 458 (1965).
- [37] P. Federman and S. Pittel, *Phys. Rev. C* **20**, 820 (1979).
- [38] K. Heyde, P. Van Isacker, R.F. Casten and J.L. Wood, *Phys. Lett. B* **155**, 303 (1985).
- [39] F. Iachello and I. Talmi, *Rev. Mod. Phys.* **59**, 339 (1987).
- [40] K. Heyde, J. Jolie, J. Moreau, J. Ryckebusch, M. Waroquier, P. Van Duppen, M. Huyse and J. L. Wood, *Nucl. Phys. A* **466**, 189 (1987).
- [41] O. Scholten, F. Iachello and A. Arima, *Ann. Phys.* **115**, 325 (1978).
- [42] Evaluated Nuclear Structure Data File (ENSDF), <https://www.nndc.bnl.gov/ensdf/>.
- [43] I. Angeli and K. P. Marinova, *At. Data Nucl. Data Tables* **99**, 69 (2013).
- [44] M. Wang, G. Audi, F. G. Kondev, W. J. Huang, S. Naimi and X. Xu, *Chinese Phys. C* **41**, 030003 (2017).
- [45] S. Zerguine, P. Van Isacker and A. Bouldjedri, *Phys. Rev. C* **85**, 034331 (2012).
- [46] J. Barea and F. Iachello, *Phys. Rev. C* **79**, 044301 (2009).
- [47] N. Gavrielov, Ph.D. Thesis, The Hebrew University, Jerusalem, Israel.
- [48] F. Iachello, *Phys. Rev. Lett.* **87**, 052502 (2001).
- [49] A. Arima, F. Iachello, *Ann. Phys. (N.Y.)* **123**, 468 (1979).
- [50] J.-P. Delaroche, M. Girod, J. Libert, H. Goutte, S. Hilaire, S. Péru, N. Pillet, and G. F. Bertsch, *Phys. Rev. C* **81**, 014303 (2010).
- [51] H. Mei, J. Xiang, J.M. Yao, Z.P. Li and J. Meng, *Phys. Rev. C* **85**, 034321 (2012).